Optimal Endobronchial Ultrasound Strain Elastography Assessment Strategy: An Explorative Study

Online Data Supplement

Roel L.J. Verhoeven[a-c], Chris L. de Korte[a-b] and Erik H.F.M. van der Heijden[c].

a. Medical Ultrasound Imaging Center (MUSIC), Radboud University Medical Center, Nijmegen, The Netherlands.
b. Faculty of Science and Technology, Twente university, Enschede, The Netherlands.
c. Department of Pulmonology, Radboud University Medical Center, Nijmegen, The Netherlands.

Corresponding Author: Erik H.F.M. van der Heijden MD, PhD, Department of Pulmonary Diseases, Radboud university Medical Center, P.O.Box 9101, 6500 HB Nijmegen (614), The Netherlands, E-mail: erik.vanderheijden@radboudumc.nl, Phone: +31 24 3610325

Technical introduction

Endobronchial ultrasound strain elastography is an ultrasound technique giving information on soft tissue by deriving elastic properties in real time. As Ying et al. and others state in their studies, the elastic modulus of lymph nodules were found to be correlating with tumour malignancy and could be measured by means of strain elastography [1–3]. Several pilot reports on use of these commercial techniques in EBUS have shown promising results [4–11]. To be able to reconstruct a strain image, backscattered signals of the tissue at a first acquisition (pre-deformation) are compared to a second acquisition (post-deformation). The time shift between the tissue reflections is then found by a cross-correlation method. Since the speed of sound is considered to be constant, this time delay estimate can be transformed into a tissue displacement. When the displacement at every depth is known, a finite difference of these displacement estimates can be used to determine the relative deformation along the imaging line, also known as axial strain [12]. Due to technical limitations of ultrasound systems, real-time strain is hard to determine in the lateral scanning direction [13]. Strain elastography is thus described as being an axial deformation and strain measurement only, different in origin than that of other reported B-mode US features [14]. All major ultrasound manufacturers such as Hitachi, Philips, Siemens Toshiba and General Electric have now commercialized strain elastography [15–17]. Although these manufacturers differ in detailed approach, the basics are similar.
In this digital supplement additional considerations for using ultrasound elastography as clinical diagnostic tool in EBUS are given together with complementary (clinical) information to the article. We furthermore introduce a standardized operating procedure for strain elastography assessment for clinical use and research for further validation of the strain elastography technique.

Materials and methods

For acquisition of images and performing measurements in this explorative study, the Hitachi Preirus Hi Vision processor (Hitachi Corporation, Tokyo, Japan) with Hitachi Real Time Elastography (version EZU-TE5) and strain histogram software (version EZU-TESH1) installed were used in combination with Pentax medical - Ultrasound Video Bronchoscopes EB-1970UK (Pentax Medical, Tokyo, Japan). A schematic flowchart of the measurement acquisition protocol can be found in Figure E.1.

Qualitative evaluation

In the image settings used, blue corresponds to relatively stiff tissue, red corresponds to relatively soft tissue and green has intermediate stiffness (see Figure 1). The VAS-scoring systems were used by the observer for subjectively quantifying or categorizing the visualized strain in the lymph node by means of its color overlay and its pattern. In the first VAS-scoring method, the observer quantifies the observed major color component of the strain image overlay. One or even two color components can be selected if the lesion was found heterogeneous in color.

The second VAS-scoring method is slightly different and is a modified scoring system for breast lesions, where it showed good potential. This so-called Tsukuba score [18] was modified by the authors to cope with the difference in tissue composition and origin of compression in breast and endobronchial applications (see Figure 2).

Semi-Quantitative EBUS-SE evaluation

A measurement technique here termed strain elastography histogram quantifies relative strain of a hand-selected region inside the lymph node into a histogram of strain counts. Through relaying strain inside this Region Of Interest (ROI) to the remainder of the image, a semi-objective measurement is obtained. This is performed by using the integral HI-RTE software as accessible on the Hitachi Preirus Hi Vision ultrasound processor. The lymph node could be selected as ROI through hand-selection of a rectangular region in the frozen dual B-mode and elastography image by the operator (see Figure 1). After measuring, the HI-RTE software provides histogram and strain information data describing the ROI area image.

A second semi-quantitative assessed scoring technique is the strain ratio. The strain ratio technique was calculated after completion of the EBUS procedure using MATLAB image post-processing software (version 9.1.0., Mathworks, Inc., Natick, MA, USA). In each case the rectangular drawn lymph node ROI as selected by the prospectively selected strain histogram scoring method was compared against a single retrospectively free-hand selected ellipsoid reference tissue area which was judged to be most suitable as reference tissue area by author R.L.J.V. (see Figure E.2). By dividing the mean strain of both areas, a ratio was found. Retrospective reference tissue area selection was performed by author R.L.J.V. on captured images, while taking into account technical and clinical boundary conditions as much as possible. During scoring, R.L.J.V. furthermore scored the selection of reference tissue upon adequacy when taking into account technical and clinical boundary conditions. Based on these conditions selecting adequate reference tissue was reported qualitatively as being difficult in 50% of cases. Reported causes were diverse, such as a lack of homogeneous reference tissue, depth

dependency artefacts, or, too small regions of interest for obtaining a single adequate secondary measurement.

Technical limitations in EBUS-SE & potential sources of artefacts

The stress that is applied to create a deformation in EBUS strain elastography was created by the patient's own pulsating heart and vasculature, as manual palpation by means of the EBUS endoscope is impossible. The amount and direction of force of these deformation sources are unknown, as they are both patient and location dependent. Given the lymph nodal map [19], it is however derived that axial strain imaging is possible by using the pulsating vasculature found distal to the EBUS transducer, with the lymph node in between source and transducer. The scoring of strain elastography is stated to be relative, since the force applied to obtain strain is unknown. The software of the different commercial systems therefore normalize the strain in every image for both visualization and calculation. This means the axial strain is semi-quantitative and will cover the entire visualized/calculated elasticity spectrum. By doing so, it relays how much strain is measured inside the region of interest when compared to surrounding tissue. When performing in-vivo imaging of mediastinal lymph nodes, several potential pitfalls and artefacts that are a consequence of the technical background of strain elastography imaging were found and are summarized below (also see [12,20–22]).

Anatomical structures - In EBUS strain elastography we ought to use the distal pulsating vasculature as source of stress only. One should assess if the lymph node itself is also invaded by vasculature, cysts, lymphatic structures or necrosis by using B-mode and Doppler. These structures add additional sources of strain or alternatively, are easily deformed and affect axial strain imaging accuracy [23]. If several structures in or out of plane are found, the possibility of using strain elastography should be reconsidered.

Amount of (axial) deformation - The amount of tissue deformation and movement influences the quality of the strain measurement. Some cases of highly enlarged pathological lymph nodes act as additional spring load and prevent sufficient deformation for quantification by the ultrasound system. This is recognizable by a generalized lack of strain rate graph amplitude (low strain). Alternatively, too much tissue displacement (>5%) [24–26] or non-axial displacement disables the underlying algorithm to correlate deformation in subsequent images. Inaccurate findings can be recognized by a non-periodical and chaotic strain image and strain rate graph with high amplitude and/or a temporally incoherent visualized strain (for a strain rate graph example, also see the lower left of each panel in Figure 1). In this explorative study a variety of cases where pulsatile forces caused overall tissue movement were found. Patient or transducer movement also

caused measurements to be aborted in several cases if applying suction or relocating the transducer did not improve imaging.

Energy absorption - As a resultant of energy absorption and spherical dissipation, the deformation obtained through applied stress decreases further away from the deformation source. The majority of (non-linear) deformation is absorbed relatively near to the stress source. For measurement reproducibility, a ROI should therefore include mediastinal tissue together with the mediastinal lymph node, but exclude the direct vicinity of the strain source (i.e. pulsating vasculature). This holds for both visualizing strain as for scoring strain, as non-linearity of scoring is potentially introduced otherwise. Last but not least, one should consider that the signal to noise ratio of the system becomes lower at increasing depth, giving rise to less accurate derivations [13,22,25].

Region of interest size - As stated earlier, measured strain values are normalized over the chosen visualized region of interest. Sufficient reference tissue should be included in visualization to give an accurate representation of relative strain. As Ciurea et al. and Havre et al. state, lesions were rated softer if the ROI for calculating strain was chosen too small relative to the lesion [21,27]. To have an adequate sized reference region, Havre et al. suggests to make the ROI size such that the lesion will be 25-50% of total ROI size [21]. Based upon our experience, we suggest to use this rule of thumb conservatively, with 25% or less being a better estimate than 50%.

Software presets - Initial software set-up of the ultrasound processing system and variation in measurement technique determine reproducibility and accuracy of lesion scoring [21]. The visualized strain is a relative measure. In relaying the relative strain information back to the user, visualization can be arbitrary. However, by changing software settings and thus visualization, efforts to quantify strain are also affected. In using strain elastography in clinical practice, both the imaging protocol for performing EBUS strain elastography as the software settings should be standardized. This is applicable both in strain visualization as in performing measurements through all scoring methods.

Supplementary results

EBUS-SE cut-off value assessments

The ideal cut-off value of the different EBUS strain elastography scoring methods was assessed in a randomly determined 80% subset of measurements using Receiver Operator Curve-plots and analysis of predictive values sensitivity, specificity, PPV, NPV and accuracy. The difference of pre- to post-test probability of malignancy using these cut-off values was calculated by the likelihood ratios as given in Table E.2. The Receiver

Operator Curve plot given by Figure E.5 also reflect the trade-off of sensitivity to specificity in the continuous semi-quantitative scores strain ratio and strain histogram. As reflected by an area under the curve of 0.637 in the Strain Ratio scoring method, performance of the strain ratio is less than that of the strain histogram method, which has an area under the curve of 0.846. The distribution of malignant to benign lesions along the different scores of the qualitative VAS methods in the training dataset can be found in the bar plots of Figure E.3-4. Both VAS scores show a sharp decline in malignancy prevalence if the scoring does not involve a majority of lymph node tissue being blue (Color VAS score Blue & Blue and green, mod. Tsukuba score 4 & 5). It furthermore stands out that the score X in the modified Tsukuba method was used in five artefactual cases of measurements, whereas this was not possible in the color VAS score, and lymph nodes as such will have been rated otherwise.

B-mode ultrasound features and PET/CT results

Ultrasound B-mode features were collected simultaneously with strain elastography measurements. Analysis of the prospectively collected B-mode characteristics are summarized in Table E.1. PET-avidity and CT based lymph nodal size results as reported by the radiologist [28] are summarized in Table E.2. B-mode analysis of predictive values gives several insights. For example, a round shape has high NPV and sensitivity (both 93%). Yet, its low specificity (51%) and PPV (53%) implies that lymph node roundness is also frequently found among non-malignant lymph nodes. Similar results can be seen for the features Central Hilar Structure (CHS) and Central Necrosis Sign (CNS). In the case of ultrasound based lymph node size and echogenicity, these predictive outliers are not found, even though a respective AUC of 73% and overall accuracy of 71% do implicate there is a relationship with malignancy. Lymph node margin on the other hand does not seem to have any predictive value at all. These results are again partially in conflict with other reported findings [29–32].

Supplementary references

1 Ying L, Hou Y, Zheng H-M, Lin X, Xie Z-L, Hu Y-P. Real-time elastography for the differentiation of benign and malignant superficial lymph nodes: a meta-analysis. Eur J Radiol 2012;81:2576–84.

2 Evans A, Whelehan P, Thomson K, McLean D, Brauer K, Purdie C, et al. Quantitative shear wave ultrasound elastography: initial experience in solid breast masses. Breast cancer Res 2010;12:R104.

3 Miyaji K, Furuse A, Nakajima J, Kohno T, Ohtsuka T, Yagyu K, et al. The stiffness of lymph nodes containing lung carcinoma metastases: a new diagnostic parameter measured by a tactile sensor. Cancer 1997;80:1920–5.

4 García FA, Ángela C, Clemente C, Santos S, Barroso ÁB, Gallego H, et al. Initial Experience With Real-Time Elastography Using an Ultrasound Bronchoscope for the Evaluation of Mediastinal Lymph Nodes. Arch Bronconeumol 2015;51:9–12.

5 He H-Y, Chen J-L, Ma H, Zhu J, Wu D-D, Lv X-D. Value of Endobronchial Ultrasound Elastography in Diagnosis of Central Lung Lesions. Med Sci Monit 2017;23:3269–3275.

6 Inage T, Nakajima T, Yoshida S, Yoshino I. Endobronchial elastography in the evaluation of esophageal invasion. J Thorac Cardiovasc Surg 2015;149:576–577.

7 Korrungruang P, Boonsarngsuk V. Diagnostic value of endobronchial ultrasound elastography for the differentiation of benign and malignant intrathoracic lymph nodes. Respirology 2017;22:972–977.

8 Okasha H, Elkholy S, Sayed M, El-Sherbiny M, El-Hussieny R, El-Gemeie E, et al. Ultrasound, endoscopic ultrasound elastography, and the strain ratio in differentiating benign from malignant lymph nodes. Arab J Gastroenterol 2018;19:1–9.

9 Izumo T, Sasada S, Chavez C, Matsumoto Y, Tsuchida T. Endobronchial Ultrasound Elastography in the Diagnosis of Mediastinal and Hilar Lymph Nodes. Jpn J Clin Oncol 2014;6:1–7.

10 Rozman A, Malovrh MM, Adamic K, Subic T, Kovac V, Flezar M. Endobronchial ultrasound elastography strain ratio for mediastinal lymph node diagnosis. Radiol Oncol 2015;49:334–340.

11 Dietrich CF, Săftoiu A, Jenssen C. Real time elastography endoscopic ultrasound (RTE-EUS), a comprehensive review. Eur J Radiol 2014;83:405–14.

12 Shiina T, Nitta N, Ueno E, Bamber J. Real time tissue elasticity imaging using the combined autocorrelation method. J Med Ultrason 2002;29:119–128.

13 Ophir J, Cespedes I, Ponnekanti H, Yazdi Y, Li X. Elastography: a quantitative method for imaging the elasticity of biological tissues. Ultrason Imaging

1991;0161–7346:111–134.
14 Fujiwara T, Yasufuku K, Nakajima T, Chiyo M, Yoshida S, Suzuki M, et al. The utility of sonographic features during endobronchial ultrasound-guided transbronchial needle aspiration for lymph node staging in patients with lung cancer: A standard endobronchial ultrasound image classification system. CHEST 2010;138:641–647.
15 Siemens healthineers. eSie Touch Elasticity imaging [cited 2018 Apr 18];Available from: http://usa.healthcare.siemens.com/ultrasound/tissue-strain-analytics
16 General Electric Company. GE Healthcare - Products - LOGIQ E9 VIDEO: Elastography [cited 2018 Apr 18];Available from: http://www3.gehealthcare.com/en/products/categories/ultrasound/logiq/logiq_e9/video_elastography
17 Hitachi Medical Systems. Hitachi Medical Systems products: Hi Vision Preirus [cited 2018 Apr 18];Available from: http://www.hitachi-medical-systems.be/products-and-services/ultrasound/platforms/hi-vision-platforms/hi-vision-preirus.html
18 Itoh A, Ueno E, Tohno E, Kamma H. Breast Disease: Clinical Application of US Elastography for Diagnosis. Radiology 2006;239:341–350.
19 Rusch V, Asamura H, Watanabe H, Giroux D, Rami-Porta R, Goldstraw P. The IASLC lung cancer staging project: a proposal for a new international lymph node map in the forthcoming seventh edition of the TNM classification for lung cancer. J Thorac Oncol 2009;4:568–577.
20 Shiina T, Nightingale KR, Palmeri ML, Hall TJ, Bamber JC, Barr RG, et al. WFUMB Guidelines and Recommendations for Clinical Use of Ultrasound Elastography: Part 3: Liver. Ultrasound Med Biol 2015;41:1161–79.
21 Havre RF, Elde E, Gilja OH, Odegaard S, Eide GE, Matre K, et al. Freehand real-time elastography: impact of scanning parameters on image quality and in vitro intra- and interobserver validations. Ultrasound Med Biol 2008;34:1638–50.
22 Kallel F, Varghese T, Ophir J, Bilgen M. The nonstationary strain filter in elastography: Part II. lateral and elevational decorrelation. Ultrasound Med Biol 1997;23:1357–1369.
23 Popescu A, Săftoiu A. Can elastography replace fine needle aspiration? Endosc ultrasound 2014;3:109–17.
24 Krouskop T, Dougherty D, Vinson F. A pulsed Doppler ultrasonic system for making noninvasive measurements of the mechanical properties of soft tissue. J Rehabil Res Dev 1987;24:1–8.
25 Parker KJ, Huang SR. Tissue response to mechanical vibrations for “sonoelasticity imaging.” Ultrasound Med Biol 1990;16:241–246.
26 Cespedes I, Ophir J, Ponnekanti H, Maklad N. Elastography: Elasticity Imaging Using Ultrasound with Application to Muscle and Breast In Vivo. Ultrason Imaging

1993;73–88.
27 Ciurea AI, Dumitriu D, Ciortea C, Botar-Jid C, Dudea SM. Artifacts and pitfalls in breast elastoultrasonography: a pictorial essay. Med Ultrason 2008;10:93–98.
28 Boellaard R, Delgado-Bolton R, Oyen WJG, Giammarile F, Tatsch K, Eschner W, et al. FDG PET/CT: EANM procedure guidelines for tumour imaging: version 2.0. Eur J Nucl Med Mol Imaging 2014;42:328–354.
29 Satterwhite LG, Berkowitz DM, Parks CS, Bechara RI. Central intra-nodal vessels to predict malignancy during EBUS-TBNA. J Bronchol Interv Pulmonol 2011;18:322–328.
30 Wang Memoli JS, El-Bayoumi E, Pastis NJ, Tanner NT, Gomez M, Huggins JT, et al. Using endobronchial ultrasound features to predict lymph node metastasis in patients with lung cancer. CHEST 2011;140 (6):1550–1556.
31 Garcia-Olivé I, Monsó E, Andreo F, Sanz J, Castellà E, Llatjós M, et al. Sensitivity of Linear Endobronchial Ultrasonography and Guided Transbronchial Needle Aspiration for The Identification of Nodal Metastasis in Lung Cancer Staging. Ultrasound Med Biol 2009;35:1271–1277.
32 Evison M, Morris J, Martin J, Shah R, Barber P V, Booton R, et al. Nodal staging in lung cancer: a risk stratification model for lymph nodes classified as negative by EBUS-TBNA. J Thorac Oncol 2015;10:126–33.

Supplementary Tables and Figures

Table E.1 – Ultrasound B-mode features for predicting mediastinal lymph node malignancy.

US B-mode features	Sens.	Spec.	PPV	NPV	Acc. (95% CI)	LR+ (95% CI)	LR- (95% CI)
SA Size >10mm	60%	68%	53%	74%	65% (56%-73%)	1.88 (1.25-2.90)	0.59 (0.37-0.84)
Shape	93%	51%	53%	93%	67% (57%-75%)	1.89 (1.50-2.46)	0.13 (0.00–0.32)
Margin	13%	79%	27%	60%	54% (45%-63%)	0.63 (0.20–1.41)	1.10 (0.92-1.29)
Echogenicity	64%	75%	60%	78%	71% (62%-79%)	3.65 (2.19-7.14)	0.43 (0.26-0.62)
CHS	98%	13%	41%	100%	46% (37%-55%)	1.15 (1.03-1.25)	0.03 (0.00–0.46)
CNS	16%	97%	78%	66%	67% (57%-75%)	5.83 (1.56-Inf)	0.87 (0.73-0.96)

Performance analysis of US B-mode features to predict the presence of mediastinal lymph node malignancy; B-mode ultrasound features were scored and selected as introduced by Fujiwara et al. (2010) [14] using the complete dataset (n=120 lymph nodes). ROC – Area under the curve of ultrasound based SA size was 0.73. The 95% CI of the accuracy and LR+ and LR- are placed between brackets. SA: Short Axis, LR+: Positive Likelihood Ratio, LR-: Negative Likelihood Ratio, Inf: Infinity.

Table E.2. - Likelihood ratios of known predictors of malignancy.

Likelihood ratios of known predictors of malignancy	Positive Likelihood Ratio (95% CI)		Negative Likelihood Ratio (95% CI)	
	Training dataset	*Validation dataset*	Training dataset	*Validation dataset*
Color VAS-system	*3.26 (2.02 – 5.66)*	*3.25*	*0.34 (0.17 – 0.54)*	*0.00**
Mod. Tsukuba Score	*4.14 (2.63 – 7.44)*	*2.60**	*0.167 (0.05 – 0.33)*	*0.00**
Strain histogram mean	*3.81 (2.52 – 6.40)*	*3.25*	*0.10 (0.00 – 0.24)*	*0.00*
Strain ratio	*3.10 (1.66 – 6.71)*	*1.86*	*0.60 (0.40 – 0.80)*	*0.84**
	Overall dataset			
Color VAS-system	*3.24 (2.17 – 5.31)*		*0.29 (0.14 – 0.47)*	
Mod. Tsukuba Score	*3.70 (2.52 – 5.99)*		*0.15 (0.04 – 0.29)*	
Strain histogram mean	*3.68 (2.55 – 5.74)*		*0.09 (0.00 – 0.21)*	
Strain ratio	*2.92 (1.60 – 5.82)*		*0.64 (0.45 – 0.82)*	
PET avid	*1.79 (1.43 – 2.31)*		*0.142 (0.00 – 0.34)*	
CT-scan ≥10 mm	*2.13 (1.63 – 2.88)*		*0.158 (0.04 – 0.34)*	
PET avid and/or CT-scan ≥10 mm	*1.42 (1.20 – 1.70)*		*0.141 (0.00 – 0.42)*	
PET avid and/or CT-scan ≥10 mm, then elastography	*4.61 (2.98 – 8.13)*		*0.143 (0.04 – 2.81)*	
PET non-avid and CT-scan ≤10 mm, then elastography	*1.35 (1.18-1.57)*		*0 (0.00-0.27)*	

Likelihood ratios and their 95% confidence intervals between brackets as calculated with given predictive values sensitivity, specificity, NPV and PPV and Bayesian statistics. The post-test probabilities as displayed in Table 2 & Table E.3 are conferred by these likelihood ratios. * Outside 95% CI as derived in training dataset.

Table E.3. Performance analysis of malignancy predicting variables

Known predictors of malignancy	N	Sens.	Spec.	PPV	NPV	Accuracy (95% CI)	Negative post-test probability of malignancy (95% CI)	Positive post-test probability of malignancy (95% CI)
PET (pos/neg)	117	93%	48%	52%	92%	65% (56-74%)	0.079 (0.00–0.17)	0.52 (0.46–0.58)
CT-scan (≥10/<10mm)	119	91%	57%	56%	91%	70% (60-78%)	0.087 (0.02–0.17)	0.56 (0.49-0.63)
PET avid AND/OR CT ≥10 mm	116	95%	33%	46%	92%	56% (46-65%)	0.078 (0.00–0.20)	0.46 (0.42–0.51)
PET avid AND/OR CT ≥10 mm AND mean strain*	90	88%	81%	73%	92%	63% (76-90%)	0.079 (0.02–0.14)	0.73 (0.64–0.83)
PET non-avid AND CT <10 mm AND mean strain†	26	100%	26%	44%	100%	53% (44-63%)	0 (0.00–0.14)	0.45 (0.41–0.49)

Performance analysis of CT and FDG-PET scan features using the complete dataset (N = 120 lymph nodes, prevalence of malignancy = 0.375) and the effect of adding EBUS-SE strain histogram mean score to PET and CT characteristics. The FDG-PET avidity as scored by the radiologists were obtained and evaluated following the European Association of Nuclear Medicine guidelines to guarantee high quality of performing, interpreting and reporting FDG-PET/CT-scans [28]. For assessing the added value of strain elastography to these predictive values, the strain histogram mean scoring method was used. Interpretation of combined results is as follows: if FDG-PET and/or CT-scan shows suspicious, being bigger than 10mm or PET avid, it is considered a positive test. If none of both applies (<10mm and FDG-PET negative), it is considered a negative test. By adding strain histogram mean scoring to either a positive test * (N = 90) or negative test † (N=26), the added value of strain elastography in clinical work-up can be exploratively assessed (Figure 4).

.

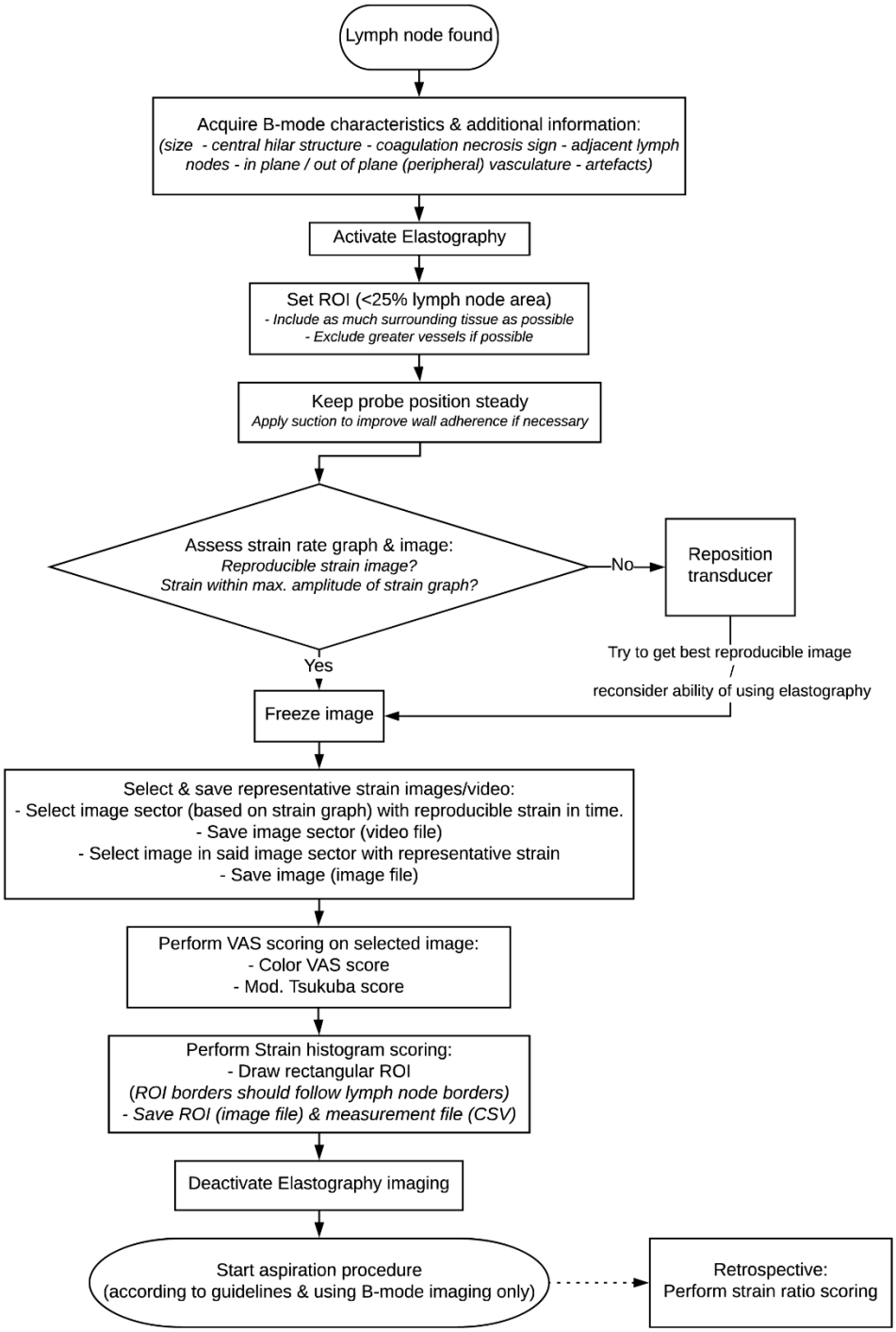

Figure E.1 – Summarized measurement acquisition protocol for obtaining reproducible strain elastography measurements.

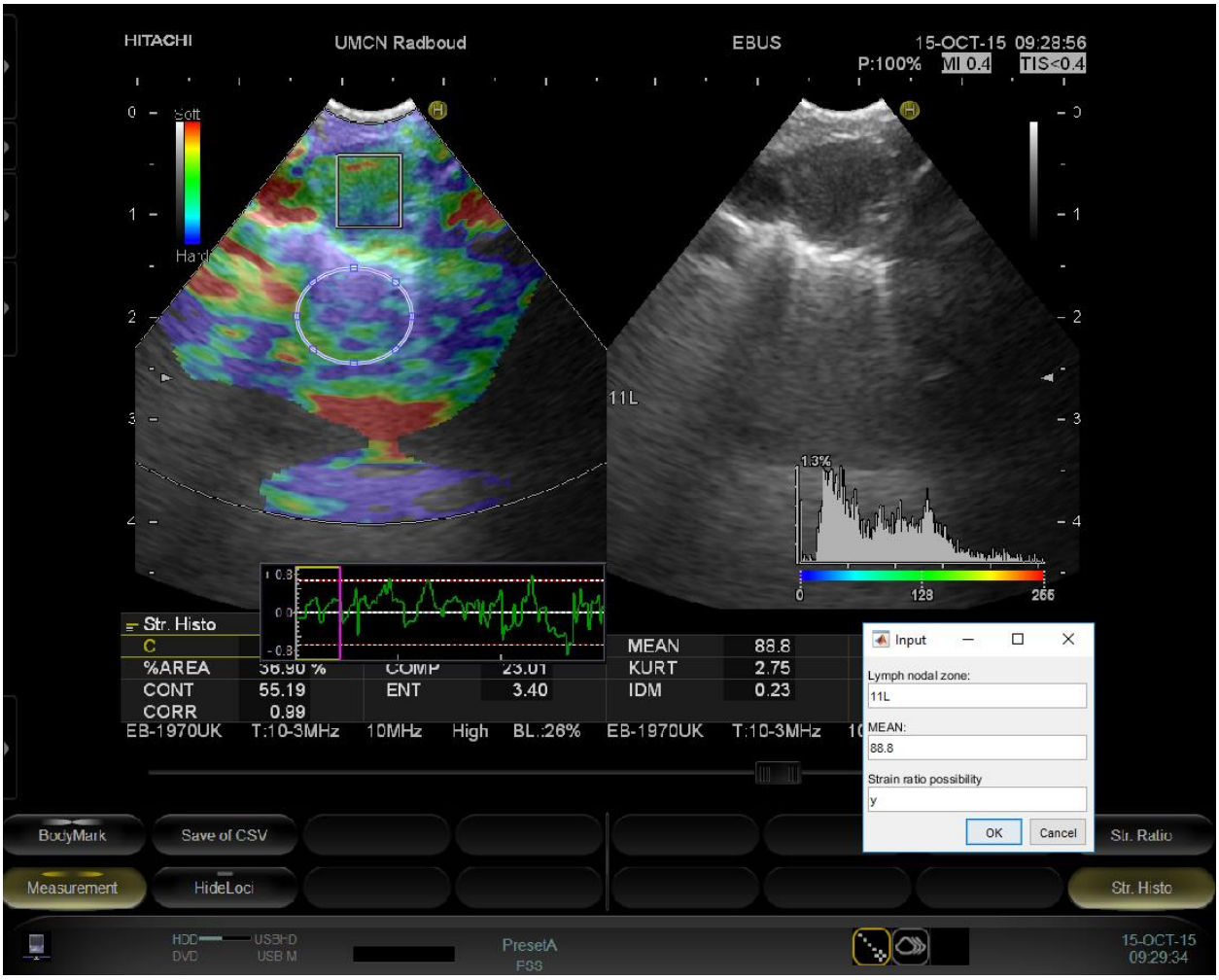

Figure E.2 - Visualization of user interface as programmed with Matlab for post procedure strain ratio extraction. The original prospectively selected rectangular region of interest for calculating the strain histogram was automatically segmented and used to compare a retrospectively selected ellipsoid reference tissue region of interest. An input dialogue was additionally used for qualitative rating of the ability to select an adequate ellipsoid reference tissue region of interest. After extraction of the region of interest selection in the original image, image masks were created. The original image was subsequently processed. Strain values were retrospectively obtained by subtraction of grey values in the RGB image. By convolving the image masks with the color-mapped image, strain values of both regions were obtained. The reference and lymphoid selection could subsequently be divided to obtain a strain ratio.

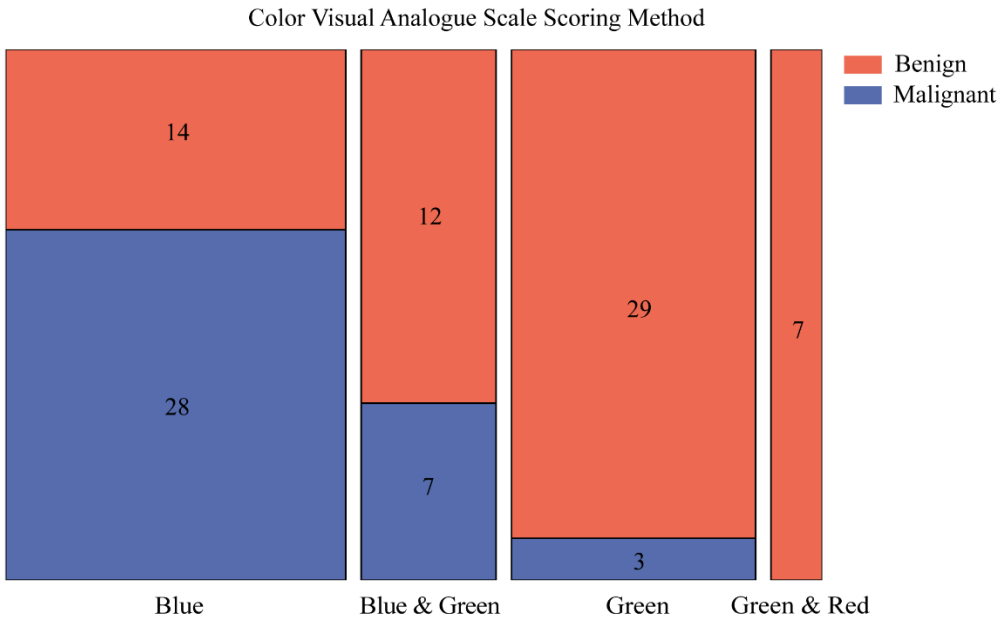

.

Figure E.3 - Distribution of malignancies and normal lymph nodes along the qualitative Color VAS scoring method. The width of column corresponds to amount of measurements as proportion of total (training dataset, n = 100). The count of measurements are also superimposed on the columns of every score.

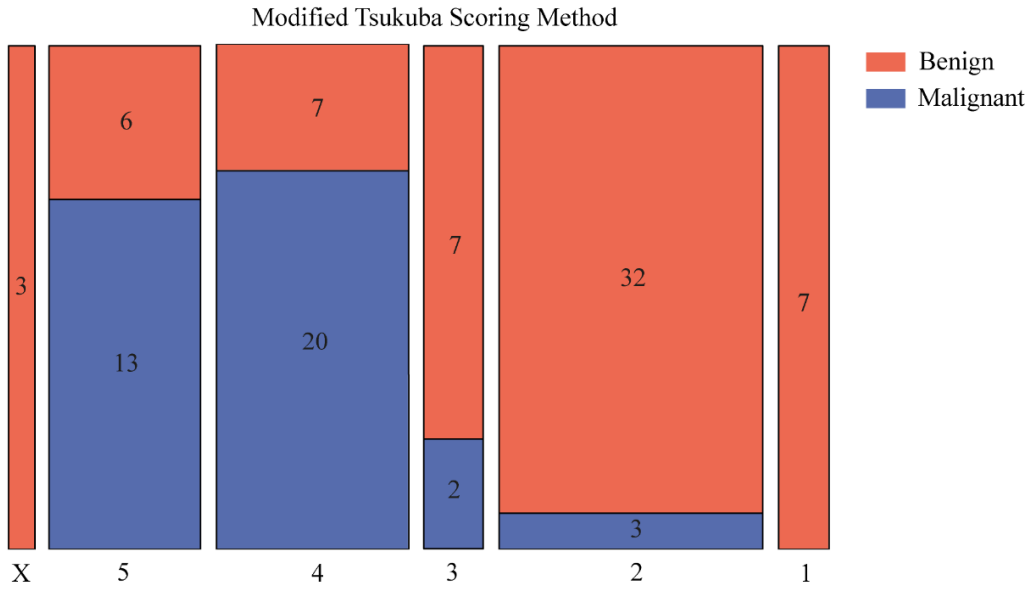

Figure E.4 - Distribution of malignancies and normal lymph nodes along the qualitative modified Tsukuba scoring method. The width of column corresponds to amount of measurements as proportion of total (training dataset, n = 100). The count of measurements are also superimposed on the columns of every score

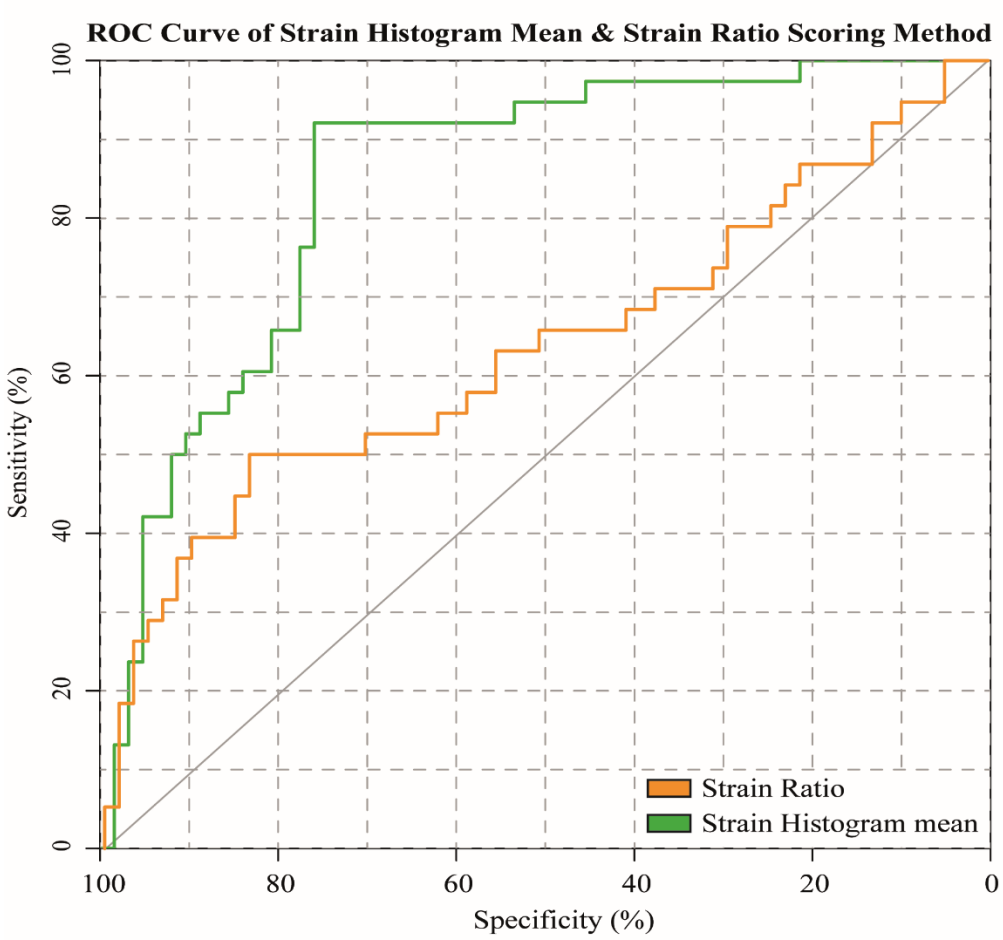

Figure E.5 - Receiver Operator Characteristic curve of strain ratio and mean of strain histogram, based on the training dataset. Area under the curve of the strain histogram mean is 0.846. Area under the curve of the strain ratio is 0.637. The top most left in both figures correspond to cut-off values of <78 and >1.67 for the strain histogram mean and strain ratio to predict malignancy, respectively. In these cases, the strain histogram mean has 92% sensitivity and 76% specificity while the strain ratio has 84% specificity and 50% sensitivity.